Hydrothermal syntheses and crystal structures of new layered tungsten(VI) methylphosphonates, $M_2(WO_3)_3PO_3CH_3$ (M = NH_4, Rb, Cs)

William T. A. Harrison,[†a] Laurie L. Dussack,[a] John T. Vaughey,[‡a] Thomas Vogt[b] and Allan J. Jacobson[a]

[a]*Department of Chemistry, University of Houston, Houston, Texas 77204-5641, USA*

[b]*Physics Department, Brookhaven National Laboratory, Upton, New York 11973, USA*

The hydrothermal syntheses of $Cs_2(WO_3)_3PO_3CH_3$, $Rb_2(WO_3)_3PO_3CH_3$ and $(NH_4)_2(WO_3)_3PO_3CH_3$, three new non-centrosymmetric, layered tungsten(VI)-containing phases, are described. The crystal structures of $Cs_2(WO_3)_3PO_3CH_3$ and $(NH_4)_2(WO_3)_3PO_3CH_3$ were refined by using Rietveld analysis of powder diffraction data. These phases are built up from hexagonal tungsten-oxide-like layers of vertex-sharing WO_6 groups, capped by P—CH_3 entities (as methylphosphonate groups) on one side of the tungsten/oxide layer. Caesium, rubidium or ammonium cations provide interlayer charge compensation for the anionic layers. IR, Raman and thermogravimetry (TG) data for these phases are also presented. Crystal data: $Cs_2(WO_3)_3PO_3CH_3$, $M_r = 1055.36$, trigonal, space group $R3$ (no. 146), $a = 7.25791(9)$ Å, $c = 20.2762(4)$ Å, $V = 925.00(4)$ Å^3, $Z = 3$, $R_p = 2.37\%$, $R_{wp} = 3.12\%$ (2943 neutron powder data). $(NH_4)_2(WO_3)_3PO_3CH_3$, $M_r = 825.63$, trigonal, $R3$ (no. 146), $a = 7.22851(7)$ Å, $c = 19.3471(3)$ Å, $V = 875.48(3)$ Å^3, $Z = 3$, $R_p = 8.14\%$, $R_{wp} = 10.12\%$ (2665 X-ray powder data).

We have now reported the syntheses and structures of several new, related, non-centrosymmetric layered materials based on a hexagonal motif of corner-sharing $V^{V}O_6$, $Mo^{VI}O_6$ or $W^{VI}O_6$ octahedra.[1–5] This layer connectivity results in a characteristic array of three- and six-rings of octahedra (Fig. 1), which is also found in three-dimensionally connected phases such as hexagonal tungsten oxide (HTO), WO_3.[6] In the new layered materials, these octahedral layers are capped, either on both faces of the MO_3 layer for the vanadium systems,[1,4] or just on one side, for the molybdenum and tungsten phases.[2,3,5] Other double-capped layered phases based on the same motif were reported earlier.[7–11]

The capping species include selenium(IV) atoms (as part of pyramidal $[SeO_3]^{2-}$ selenite groups) in $NH_4(VO_2)_3(SeO_3)_2$,[1] $K(VO_2)_3(SeO_3)_2$,[4] $(NH_4)_2(MoO_3)_3SeO_3$,[2] $Cs_2(MoO_3)_3SeO_3$,[2] $(NH_4)_2(WO_3)_3SeO_3$[5] and $Cs_2(WO_3)_3SeO_3$.[5] In both $Cs_2(MoO_3)_3PO_3CH_3$[3] and $Rb_2(MoO_3)_3PO_3CH_3$,[3] P—CH_3 entities (as part of $[O_3PCH_3]^{2-}$ methylphosphonate groups) provide the capping. Alkali-metal or ammonium cations serve as the interlayer charge-balancing species in all these phases.

In this paper we report the syntheses, structures and some properties of $Cs_2(WO_3)_3PO_3CH_3$, $Rb_2(WO_3)_3PO_3CH_3$ and $(NH_4)_2(WO_3)_3PO_3CH_3$, the tungsten(VI)-containing analogues of the layered alkali-metal molybdenum (VI) methylphosphonate materials $Cs_2(MoO_3)_3PO_3CH_3$ and $Rb_2(MoO_3)_3PO_3CH_3$.[3]

Synthesis and Initial Characterization

$Cs_2(WO_3)_3PO_3CH_3$ was hydrothermally prepared from 0.873 g $CsOH{\cdot}H_2O$ (5.2 mmol Cs), 0.6 g WO_3 (2.6 mmol W), 0.5 g 98% $CH_3PO_3H_2$ (5.2 mmol P), and 12 cm^3 of H_2O (initial Cs : W : PO_3CH_3 ratio = 2 : 1 : 2). These reactants were sealed in a 23 cm^3 PTFE-lined Parr bomb and heated to 200 °C for 5 days. After overnight cooling, the pH of the final filtrate was 3.1. Fine white $Cs_2(WO_3)_3PO_3CH_3$ powder was recovered by vacuum filtration and air drying. The overall yield of solid product, based on tungsten, was *ca.* 87% by mass.

$Rb_2(WO_3)_3PO_3CH_3$ was synthesized from a mixture of 0.530 g 50% aqueous RbOH solution (2.59 mmol Rb), 0.6 g WO_3 (2.59 mmol W), 0.497 g 98% $CH_3PO_3H_2$ (5.18 mmol P) and 10 cm^3 water. The initial mole ratio of reactants was 1 : 1 : 2 Rb : W : P. The mixture was sealed in a Parr bomb, heated to 200 °C for 11 days, and allowed to cool to ambient temperature over 24 h. Fine white $Rb_2(WO_3)_3PO_3CH_3$ powder (yield = 30% based on W) was recovered from the filtrate (pH = 2.0) by vacuum filtration. Reactions with higher starting concentrations of Rb resulted in products contaminated with unreacted WO_3 (X-ray powder diffraction measurements).

The best method to prepare pure, highly crystalline $(NH_4)_2(WO_3)_3PO_3CH_3$ started from a mixture of 0.3 g $(NH_4)_{10}W_{12}O_{41}$ (1.18 mmol W), 0.38 g NH_4Cl (7.1 mmol NH_4), 0.34 g $CH_3PO_3H_2$ (3.55 mmol P), 2.85 g 35% tetra-

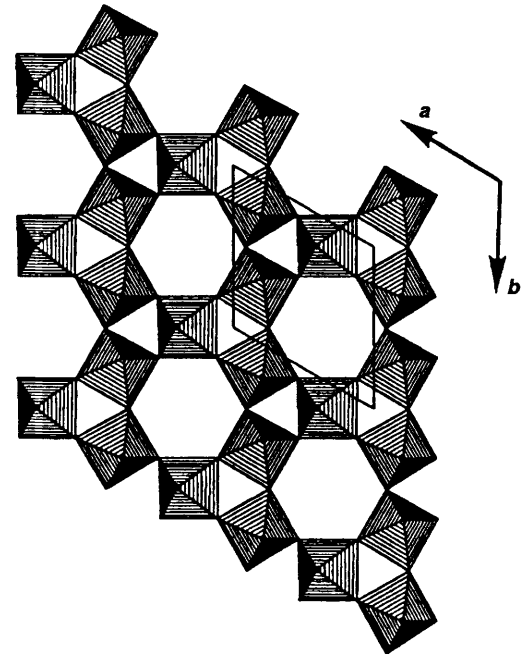

Fig. 1 STRUPLO polyhedral view of a generic hexagonal tungsten oxide (HTO) octahedral layer, viewed down the crystallographic [001] direction, showing the infinite network of octahedral 3- and 6-rings

† Present address: Department of Chemistry, University of Western Australia, Nedlands, WA 6907, Australia.

‡ Present address: Department of Chemistry, University of Iowa, Ames, Iowa 50011, USA.

ethylammonium hydroxide (TEAOH) and 6 cm^3 water. The reactants were heated to 180 °C for 5 days in a Parr bomb. Product recovery by vacuum filtration led to an 85% yield of white $(NH_4)_2(WO_3)_3PO_3CH_3$ powder (pH of filtrate = 6.6). Reactions at lower starting pHs (less TEAOH added to reaction) resulted in lower yields of $(NH_4)_2(WO_3)_3PO_3CH_3$ (*e.g.* 47% at pH 3.8).

X-Ray powder data for thoroughly ground samples of the title compounds were recorded on a Scintag XDS 2000 automated powder diffractometer [Cu-Kα radiation, $\bar{\lambda}$ = 1.54178 Å, T = 25(2) °C]. They resulted in similar powder patterns which could be indexed on rhombohedrally centred hexagonal unit cells (see Table 6, later). These R-centred unit cells suggested that $Cs_2(WO_3)_3PO_3CH_3$, $Rb_2(WO_3)_3PO_3CH_3$ and $(NH_4)_2(WO_3)_3PO_3CH_3$ are isostructural with the three-layer molybdenum-containing materials $Cs_2(MoO_3)_3PO_3CH_3$ and $Rb_2(MoO_3)_3PO_3CH_3$,[3] as was found to be the case when full profile refinements were carried out (*vide infra*).

Since we could not obtain suitably sized single crystals of these materials for X-ray diffraction measurements, we proceeded to refine their crystal structures by the Rietveld method. X-Ray data were used for $(NH_4)_2(WO_3)_3PO_3CH_3$. In order to maximize the refinement precision of the lighter atoms, neutron powder data were collected for $Cs_2(WO_3)_3PO_3CH_3$.

Crystal Structure Refinement

The crystal structure of $Cs_2(WO_3)_3PO_3CH_3$ was optimized by the Rietveld method using constant-wavelength powder neutron diffraction data. A *ca.* 10 g quantity of ground white powder sample was loaded and sealed into a cylindrical vanadium sample can. Room temperature, high-resolution powder data were collected on the HRNPD diffractometer at the High Flux Beam Reactor (HFBR), Brookhaven National Laboratory. A data collection time of 48 h resulted in satisfactory counting statistics ($5° < 2\theta < 165°$; step size = 0.05°; λ = 1.8857 Å, as precalibrated with Al_2O_3). A characteristic large background signal was observed for the $Cs_2(WO_3)_3PO_3CH_3$ sample, due to incoherent scattering from the methyl protons.

The $Cs_2(WO_3)_3PO_3CH_3$ structure refinement was carried out using the program GSAS.[12] The initial atomic model, in space group $R3$ (no. 146), was based on the structure of $Cs_2(MoO_3)_3PO_3CH_3$,[3] with W substituting for Mo. The calculated $Cs_2(MoO_3)_3PO_3CH_3$ proton position was not included in the initial refinement cycles for $Cs_2(WO_3)_3PO_3CH_3$. Coherent neutron scattering lengths ($\times 10^{-12}$ m) of b(C) = 0.665, b(H) = −0.374, b(Cs) = 0.542, b(W) = 0.477, b(P) = 0.513 and b(O) = 0.581 were assumed. The refinement proceeded in typical fashion, with profile (scale factor, detector zero-point correction, polynomial background descriptors, peak shape parameters) and atomic positional and thermal parameters added to the model as additional variables as the refinement converged. The single crystallographic proton site was located from a difference Fourier synthesis, and added to the atomic model as an H atom. A simple Gaussian model was found to be inadequate to describe the observed peak shape, and a significantly better fit was obtained by using a pseudo-Voigt Gaussian/Lorentzian model.[13]

The structure of $(NH_4)_2(WO_3)_3PO_3CH_3$ was refined by the Rietveld method using powder X-ray data (Scintag XDS5000, flat-plate sample geometry, θ–θ geometry, $20° < 2\theta < 100°$). The starting model for $(NH_4)_2(WO_3)_3PO_3CH_3$ in space group $R3$ (no. 146) was taken from that of $Cs_2(WO_3)_3PO_3CH_3$ (N replacing Cs). The X-ray Rietveld refinement proceeded normally, and profile and atomic parameters were added to the model as variables as the refinement progressed. The refinement converged to satisfactory residuals (program: GSAS), but the precision of the refined light-atom parameters is much poorer than the equivalent values obtained from the neutron refinement on $Cs_2(WO_3)_3PO_3CH_3$. No possible $(NH_4)_2(WO_3)_3PO_3CH_3$ proton positions could be located from Fourier maps.

Table 1 Crystallographic parameters

	$Cs_2(WO_3)_3PO_3CH_3$	$(NH_4)_2(WO_3)_3PO_3CH_3$
empirical formula	$W_3Cs_2P_1O_{12}C_1H_3$	$W_3P_1O_{12}N_2C_1H_{11}$
formula mass	1055.36	825.63
habit	powder	powder
colour	white	white
crystal system	trigonal	trigonal
a/Å	7.25791(9)	7.22851(7)
c/Å	20.2762(4)	19.3471(3)
V/Å^3	925.00(4)	875.48(3)
Z	3	3
space group	$R3$ (no. 146)	$R3$ (no. 146)
T/°C	25(2)	25(2)
radiation	neutrons	X-rays
λ/Å	1.8857	1.5418
ρ_{calc}/g cm^{-3}	5.68	4.70
powder data	2943	2665
parameters refined	51	29
R_p[a] (%)	2.37	8.14
R_{wp}[b] (%)	3.12	10.12
χ^2	5.84	3.84

[a] $R_p = 100 \times \Sigma|y_0 - Cy_c|/\Sigma|y_0|$. [b] $R_{wp} = 100 \times [\Sigma w(y_0 - Cy_c)^2/\Sigma w y_0^2]^{1/2}$, where C is a scale factor.

Crystal and experimental data for these refinements are listed in Table 1. Final observed, calculated and difference profiles for the $Cs_2(WO_3)_3PO_3CH_3$ and $(NH_4)_2(WO_3)_3PO_3CH_3$ refinements are shown in Fig. 2 and 3, respectively.

Physical Measurements

Thermogravimetry (TG) data for $Cs_2(WO_3)_3PO_3CH_3$, $Rb_2(WO_3)_3PO_3CH_3$ and $(NH_4)_2(WO_3)_3PO_3CH_3$ were collected on a DuPont 2950 analyser (ramp 5 °C min^{-1} under flowing O_2 gas). The post-TG residues were analysed by powder X-ray diffraction (XRD).

IR spectra (KBr pellet method) for the title compounds were recorded in the 400–4000 cm^{-1} range on a Galaxy FTIR 5000 series spectrometer. Raman data were obtained using a coherent K-2 Kr^+ ion laser excited at 406.7 nm. Data for $Cs_2(MoO_3)_3PO_3CH_3$ (KBr pellet method) were accumulated at 1 s intervals for every wavenumber over the range 100–1700 cm^{-1} (Spex 1403 double monochromator/Hamamatsu 928 photomultiplier detection system).

Results

Crystal structures

Final atomic positional and thermal parameters for $Cs_2(WO_3)_3PO_3CH_3$ are listed in Table 2, with selected bond distance/angle data in Table 3. Similar data for $(NH_4)_2(WO_3)_3PO_3CH_3$ are listed in Tables 4 and 5 $Cs_2(WO_3)_3PO_3CH_3$ and $(NH_4)_2(WO_3)_3PO_3CH_3$ both crys-

Table 2 Atomic positional/thermal parameters for $Cs_2(WO_3)_3PO_3CH_3$

atom	x	y	z	U_{iso}/Å^2
Cs(1)	0	0	0.1733(4)	0.026(2)
Cs(2)	1/3	2/3	0.2291(5)	0.008(2)
W(1)	0.0033(9)	0.5189(13)	0.05724(26)	0.011(2)
P(1)	−1/3	1/3	0.1871(4)	0.018(2)
O(1)	0.0719(9)	0.5410(18)	−0.02355(23)	0.026(2)
O(2)	0.2201(14)	0.7921(14)	0.08817(22)	0.010(2)
O(3)	−0.2030(14)	0.5799(8)	0.05131(23)	0.006(2)
O(4)	−0.0936(7)	0.4589(13)	0.16167(23)	0.003(2)
C(1)	−1/3	1/3	0.2727(4)	0.013(2)
H(1)	0.5010(15)	0.2034(15)	0.2935(4)	0.036(3)

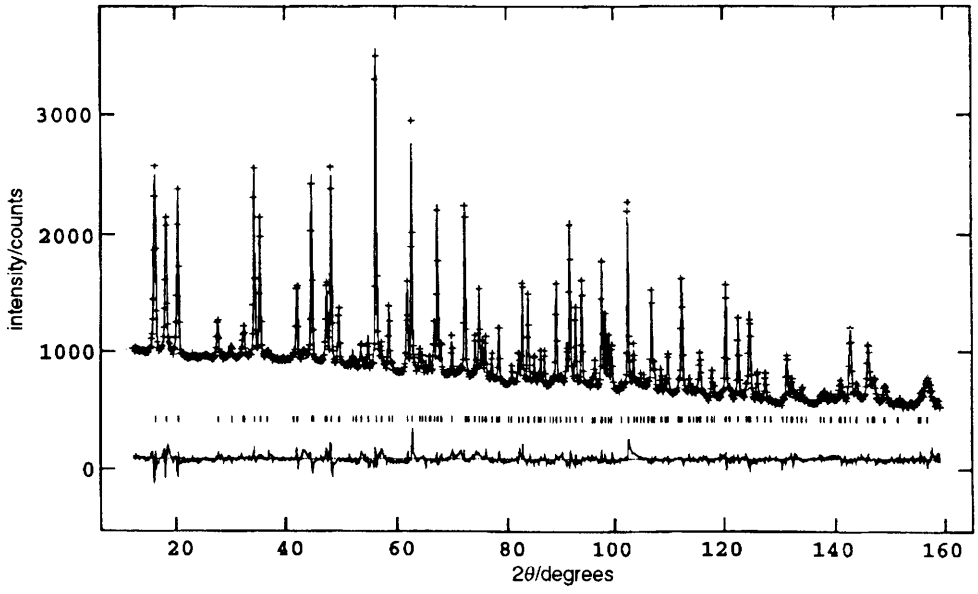

Fig. 2 Final observed (crosses), calculated (line) and difference profile plots for the Rietveld refinement of $Cs_2(WO_3)_3PO_3CH_3$ (neutron data)

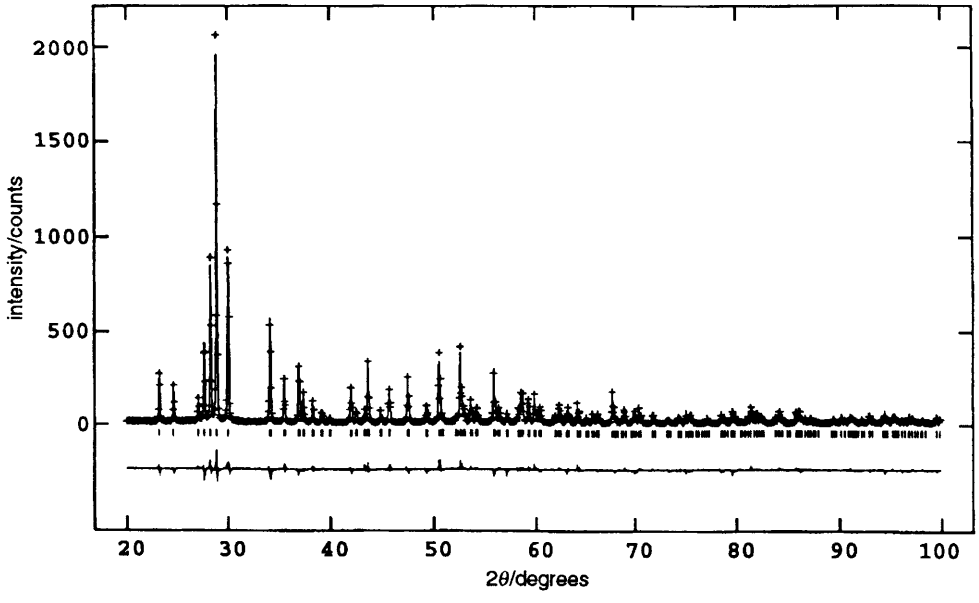

Fig. 3 Final observed (crosses), calculated (line) and difference profile plots for the Rietveld refinement of $(NH_4)_2(WO_3)_3PO_3CH_3$ (X-ray data)

tallize as isostructures of the $M_2(MoO_3)_3PO_3CH_3$ (M = Cs, Rb) structure reported earlier.[3]

This structure type consists of anionic layers of vertex-sharing WO_6 octahedra and tetrahedral PO_3CH_3 (methylphosphonate) units, which are fused together by W—O—W and W—O—P bonds. Two crystallographically distinct caesium or ammonium cations provide interlayer charge balancing. The crystal structure of $Cs_2(WO_3)_3PO_3CH_3$ is illustrated in Fig. 4–6.

The layer motif in $Cs_2(WO_3)_3PO_3CH_3$ and $(NH_4)_2(WO_3)_3PO_3CH_3$ consists of hexagonal tungsten-oxide-like sheets of vertex-sharing WO_6 octahedra. Each WO_6 unit shares four of its W—O vertices with similar neighbours [*via* 2 × O(2) and 2 × O(3)], with these W—O—W′ bonds roughly aligned in the ***ab*** plane. The W(1)—O(2) bond is canted from the ***ab*** plane by *ca.* 19°, and the W(1)—O(3) bond by *ca.* 4°. This canting of the W(1)—O(2) vertex effectively forces a 'three-ring' trio of apical W(1)—O(4) bonds closer together to allow them to be capped (see below). Three-rings and six-rings of octahedra result from this in-plane connectivity (Fig. 6). The two remaining apical W—O bonds, to O(1) and O(4), project into the interplanar region of the structure. The PCH_3 entity caps a 'three-ring' of O(4) atoms in the structure, while the O(1) atoms are uncapped, resulting in short W(1)=O(1) 'oxo' bonds. All the W—O(4)—P capping occurs on one side of the W/O sheet. Both O(2) and O(3) bridge adjacent tungsten atoms into three-rings. The overall sheet stoichiometry is $[(WO_3)_3PO_3CH_3]^{2-}$.

In $Cs_2(WO_3)_3PO_3CH_3$, the WO_6 octahedron is significantly distorted from octahedral regularity: the tungsten atom is displaced by $\Delta_{Oct} = 0.28$ Å from the geometrical centre of its six oxygen atom neighbours. This distortion may be viewed as a displacement of the tungsten atom from the centre of the WO_6 octahedron towards an octahedral edge [atoms O(1) and O(3)] (Fig. 7), which results in two short ($d < 1.8$ Å) W—O bonds, three intermediate length W—O bonds, and one long ($d > 2.2$ Å) W—O vertex. The inter-octahedral W—O(3)—W′ bonds thus show some degree of short–long bond length 'alternation', whereas the comparable W—O(2)—W′ bonds are not significantly different in length (Table 3).

The methylphosphonate group in $Cs_2(WO_3)_3PO_3CH_3$ has typical geometrical parameters (Table 3). The P and C atoms

Table 3 Bond distances (Å) and angles (degrees) for $Cs_2(WO_3)_3PO_3CH_3$

Cs(1)–O(1)×3	3.219(9)	Cs(1)–O(2)×3	3.196(7)
Cs(2)–O(1)×3	3.028(8)	Cs(2)–O(2)×3	3.228(10)
Cs(2)–O(4)×3	3.012(7)		
W(1)–O(1)	1.696(7)	W(1)–O(2)	1.919(13)
W(1)–O(2)	2.004(12)	W(1)–O(3)	1.765(10)
W(1)–O(3)	2.040(10)	W(1)–O(4)	2.205(7)
P(1)–O(4)×3	1.594(6)	P(1)–C(1)	1.735(12)
C(1)–H(1)×3	1.174(11)		
O(1)–W(1)–O(2)	99.7(5)	O(1)–W(1)–O(2)	95.9(5)
O(1)–W(1)–O(3)	99.0(5)	O(1)–W(1)–O(3)	94.4(5)
O(1)–W(1)–O(4)	174.7(8)	O(2)–W(1)–O(2)	83.0(4)
O(2)–W(1)–O(3)	97.1(4)	O(2)–W(1)–O(3)	163.3(4)
O(2)–W(1)–O(4)	84.60(31)	O(2)–W(1)–O(3)	164.9(4)
O(2)–W(1)–O(3)	86.7(4)	O(2)–W(1)–O(4)	81.37(34)
O(3)–W(1)–O(3)	89.5(4)	O(3)–W(1)–O(4)	83.59(33)
O(3)–W(1)–O(4)	80.86(31)		
O(4)–P(1)–C(1)	108.9(4)	O(4)–P(1)–O(4)	110.0(4)
W(1)–O(2)–W(1)	133.2(4)	W(1)–O(3)–W(1)	149.4(4)
W(1)–O(4)–P(1)	125.0(4)	P(1)–C(1)–H(1)	111.0(5)

Table 4 Atomic positional parameters for $(NH_4)_2(WO_3)_3PO_3CH_3$

atom	x	y	z	U_{iso}/Å^2
N(1)	0	0	0.1730	0.0088(5)
N(2)	1/3	2/3	0.229(11)	0.0088(5)
W(1)	0.0058(6)	0.5204(4)	0.064(6)	0.0088(5)
P(1)	−1/3	1/3	0.199(6)	0.0088(5)
O(1)	0.061(4)	0.547(5)	−0.021(6)	0.0088(5)
O(2)	0.223(8)	0.804(9)	0.094(6)	0.0088(5)
O(3)	−0.218(8)	0.582(4)	0.054(7)	0.0088(5)
O(4)	−0.098(4)	0.444(6)	0.165(6)	0.0088(5)
C(1)	−1/3	1/3	0.2839(29)	0.0088(5)

Table 5 Selected bond distances (Å) and angles (degrees) for $(NH_4)_2(WO_3)_3PO_3CH_3$

N(1)–O(1)×3	3.19(9)	N(1)–O(2)×3	3.04(7)
N(2)–O(1)×3	2.95(10)	N(2)–O(2)×3	3.05(15)
N(2)–O(4)×3	2.98(8)		
W(1)–O(1)	1.685(20)	W(1)–O(2)	1.94(6)
W(1)–O(2)	1.94(5)	W(1)–O(3)	1.89(6)
W(1)–O(3)	1.94(5)	W(1)–O(4)	2.062(19)
P(1)–O(4)×3	1.613(23)	P(1)–C(1)	1.64(14)
O(1)–W(1)–O(2)	98.4(15)	O(1)–W(1)–O(2)	99.2(12)
O(1)–W(1)–O(3)	93.0(13)	O(1)–W(1)–O(3)	92.0(13)
O(1)–W(1)–O(4)	171.6(16)	O(2)–W(1)–O(2)	87.7(17)
O(2)–W(1)–O(3)	96.8(6)	O(2)–W(1)–O(3)	167.6(12)
O(2)–W(1)–O(4)	90.0(13)	O(2)–W(1)–O(3)	166.3(13)
O(2)–W(1)–O(3)	83.9(7)	O(2)–W(1)–O(4)	81.6(14)
O(3)–W(1)–O(3)	89.4(16)	O(3)–W(1)–O(4)	85.5(13)
O(3)–W(1)–O(4)	79.8(12)		
O(4)–P(1)–O(4)	104.4(13)	O(4)–P(1)–C(1)	114.1(11)
W(1)–O(2)–W(1)	133.0(13)	W(1)–O(3)–W(1)	147.9(16)
W(1)–O(4)–P(1)	132.2(18)		

are on a three-fold axis, and three equivalent P(1)–O(4) bonds result, each of which bridges to a different WO_6 unit. The hydrogen atoms of the methyl group are close to being staggered with respect to the oxygen atoms of the PO_3 moiety [H(1)–C(1)–P(1)–O(4) torsion angle, $\xi = 163°$]. The methyl group points towards an octahedral six-ring in the next $[(WO_3)_3PO_3CH_3]^{2-}$ sheet, and the minimum non-bonding C–H···O separation is *ca.* 2.7 Å.

The two crystallographically distinct cation sites (both with site symmetry 3) are both found in the interlayer region for these phases. Cs(1) is six-coordinate to nearby oxygen atoms

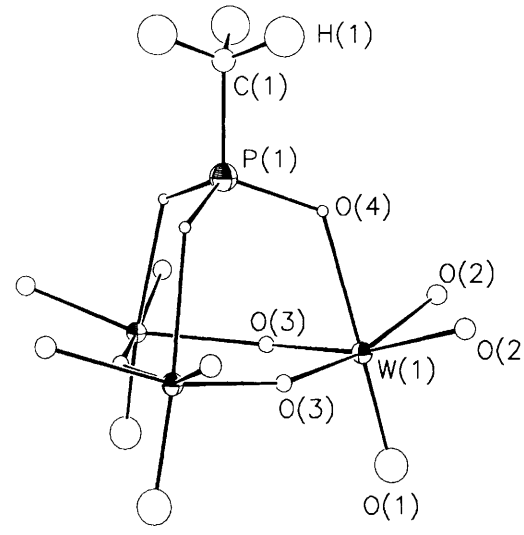

Fig. 4 ORTEP view of the WO_3/PO_3CH_3 building unit of $Cs_2(WO_3)_3PO_3CH_3$, showing the atom-labelling scheme

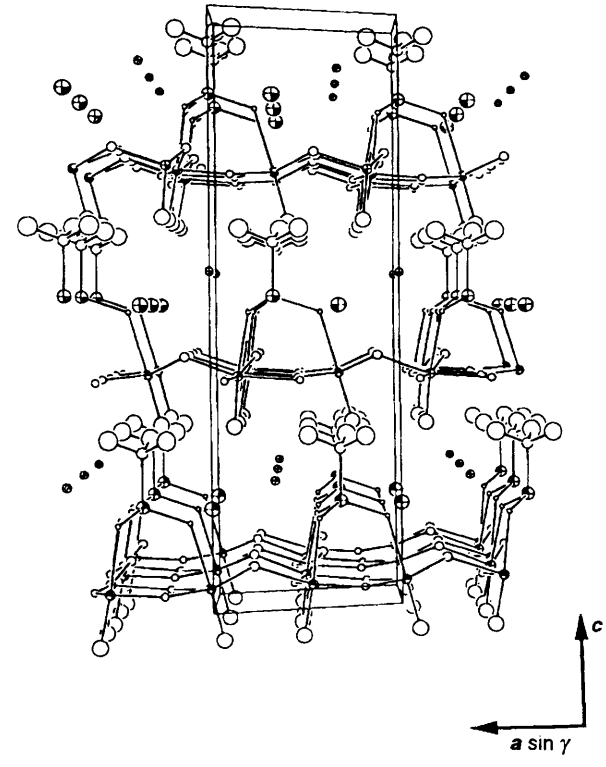

Fig. 5 View down the [010] direction of the unit-cell packing of $Cs_2(WO_3)_3PO_3CH_3$, showing the ABC ... sheet structure of $(WO_3)_3PO_3CH_3$ layers (Cs–O contacts not shown for the interlayer Cs^+ species)

and forms a distorted trigonal prism with respect to three oxygen atoms in one adjacent $(WO_3)_3PO_3CH_3$ layer, and three in the other. Cs(2) is nine-coordinate and makes six Cs–O bonds to one adjacent $(WO_3)_3PO_3CH_3$ sheet, and three Cs–O bonds to the other. Bond valence sum[14] (BVS) values for these cations {BVS [Cs(1)] = 0.78, BVS [Cs(2)] = 1.56, expected value = 1.00 in both cases} suggest that the stability of this structure type is not crucially determined by the bonding requirements (size) of the guest cation. However, these species must have some role to play in stabilizing the HTO-type six-ring windows, and must be large enough to bridge adjacent $(WO_3)_3PO_3CH_3$ layers.

The $(NH_4)_2(WO_3)_3PO_3CH_3$ structure is substantially similar to that of $Cs_2(WO_3)_3PO_3CH_3$, but the modest precision of

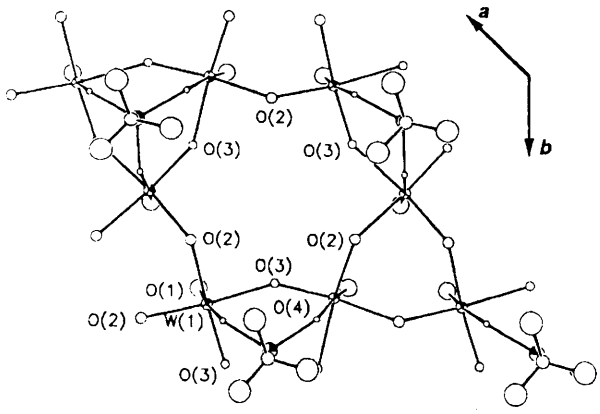

Fig. 6 View down the [001] direction of part of one $(WO_3)_3PO_3CH_3$ layer in $Cs_2(WO_3)_3PO_3CH_3$, with selected atoms labelled. The two types of 3-ring may be seen: the capped 3-ring with W atoms linked by O(3) species, and the uncapped 3-ring, with O(2) atoms forming the W—O—W bridges. O(2) and O(3) species alternate around the 6-rings (*cf.* Fig. 1).

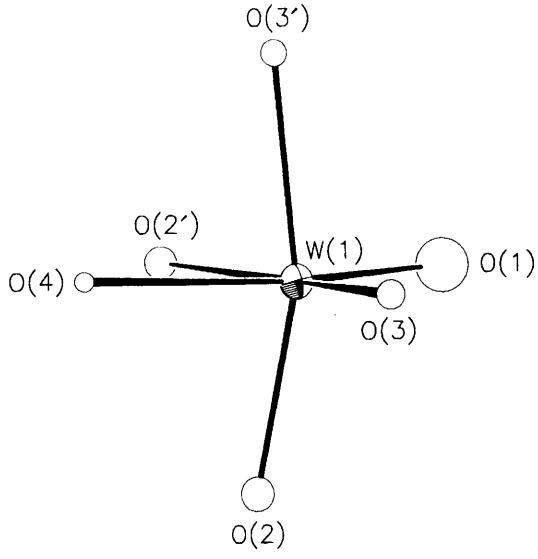

Fig. 7 Detail of the tungsten atom coordination in $Cs_2(WO_3)_3PO_3CH_3$ showing the displacement of the W atom from the geometrical centre of its octahedron towards the octahedral edge defined by atoms O(1) and O(3) (see text)

the X-ray Rietveld refinement [the esds of the derived parameters are about 4 times as large for $(NH_4)_2(WO_3)_3PO_3CH_3$ compared with those for $Cs_2(WO_3)_3PO_3CH_3$] makes more detailed comparisons difficult. It is clear that the ammonium cations in $(NH_4)_2(WO_3)_3PO_3CH_3$ occupy similar sites to their caesium counterparts in $Cs_2(WO_3)_3PO_3CH_3$. However, no details regarding the hydrogen-bonding scheme in $(NH_4)_2(WO_3)_3PO_3CH_3$, if any, could be elucidated in this study.

Physical data

TG for $Cs_2(WO_3)_3PO_3CH_3$ (oxygen atmosphere) showed a gradual 0.4% mass loss to 500 °C, then a sharp 0.6% mass loss at 600 °C. The white post-TG residue consisted of unidentified phase(s). TG for $Rb_2(WO_3)_3PO_3CH_3$ showed a slight (*ca.* 0.15%) mass loss to 530 °C, followed by a sharp loss at *ca.* 600 °C (overall loss = 1.3%). After heating to 650 °C, the post-TG residue was white; further heating to 800 °C resulted in a light-yellow phase. Powder XRD showed this yellow residue to consist of hexagonal WO_3[15] and other unidentified components. The decomposition path for $Cs_2(WO_3)_3PO_3CH_3$ is unknown: however, it is thermally stable to *ca.* 500 °C (powder XRD measurements on a post-thermally treated sample): the initial slight mass losses for $Cs_2(WO_3)_3PO_3CH_3$ and $Rb_2(WO_3)_3PO_3CH_3$ are attributable to loss of surface absorbed water, apparent from the IR results.

TG for $(NH_4)_2(WO_3)_3PO_3CH_3$ (ramp 5 °C min^{-1} to 500 °C under O_2) showed a one-step 7.6% mass loss from 350 to 475 °C. The crystalline component of the off-white residue was hexagonal WO_3. Further heating to 680 °C led to a light-yellow residue which contained both hexagonal and triclinic WO_3.[16] Heating $(NH_4)_2(WO_3)_3PO_3CH_3$ to 800 °C showed a 7.7% mass loss at 500 °C, a slight mass gain to 700 °C, and a second sharp mass loss at 700–720 °C (overall mass loss = 8.5%). The light-green residue contains crystalline triclinic WO_3 and, by implication, glassy tungsten/phosphate components.

The IR spectrum of $(NH_4)_2(WO_3)_3PO_3CH_3$ (Fig. 8) shows four characteristic NH_4 bands at 3335, 3160 and 3048 cm^{-1} (ν_1 and ν_3 modes), and a strong, sharp band at 1410 cm^{-1} (ν_4 mode). The spectra of $Cs_2(WO_3)_3PO_3CH_3$ (Fig. 9) and $Rb_2(WO_3)_3PO_3CH_3$ (Fig. 10) are featureless in these regions. All three spectra show complex, overlapping WO_6 modes in the 650–600 cm^{-1} region, and four sharp peaks which may be correlated with P—O phosphonate modes in the region between 1040 and 860 cm^{-1}. Similar bands have been seen in previous studies of metal/oxygen clusters capped by alkylphosphonate groups.[17] Small, sharp peaks at 2940 and 1415 cm^{-1} are methyl C—H bending and stretching modes, and the small

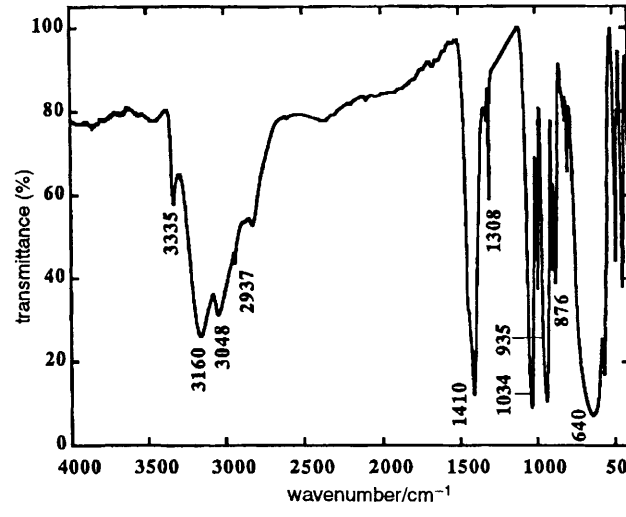

Fig. 8 IR spectrum of $(NH_4)_2(WO_3)_3PO_3CH_3$

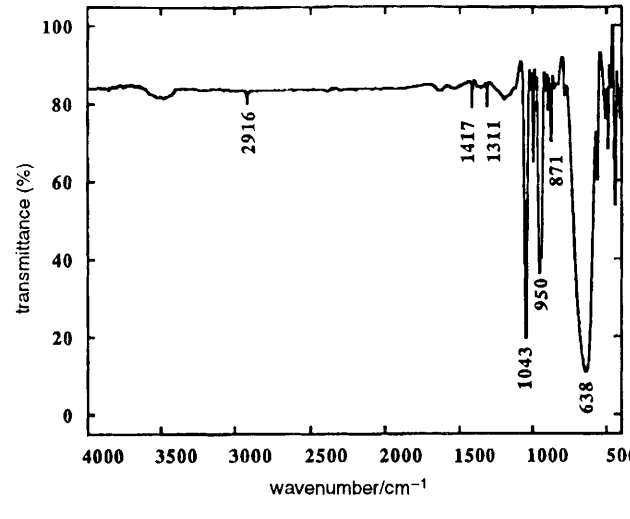

Fig. 9 IR spectrum of $Cs_2(WO_3)_3PO_3CH_3$

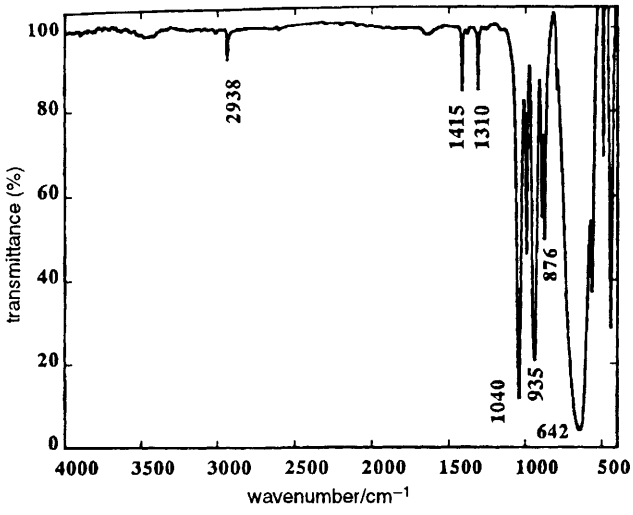

Fig. 10 IR spectrum of $Rb_2(WO_3)_3PO_3CH_3$

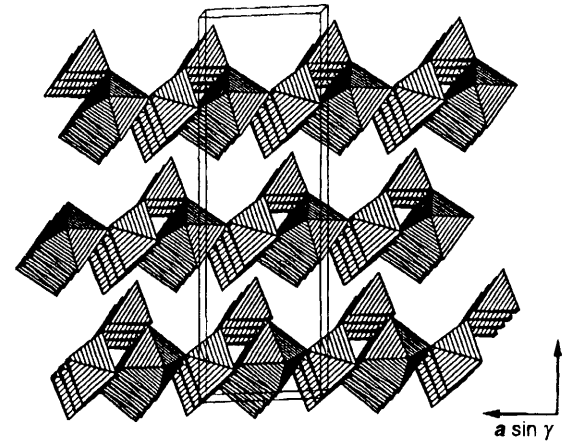

Fig. 12 Polyhedral view of the $Cs_2(WO_3)_3PO_3CH_3$ structure, viewed down the [010] direction, showing the 3-layer repeat motif of the singly capped tungsten oxide layers. Cs and H atoms are omitted for clarity.

sharp band at *ca.* 1310 cm^{-1} represents the P—C stretch, and is seen for all three samples.

The Raman spectrum of $Cs_2(WO_3)_3PO_3CH_3$ (Fig. 11) correlates well with the IR spectrum of the same compound. Strong Raman bands may be assigned to more symmetric stretching modes for the WO_6 (626, 698 cm^{-1}) and PO_3C (932, 965 cm^{-1}) groups. The weaker peaks at 1310 and 1415 cm^{-1} match the P—C and C—H modes seen in the IR spectrum. Raman bands below *ca.* 350 cm^{-1} correspond to lattice (phonon) modes as seen in related phases.[2,3,5]

Conclusions

Compounds $Cs_2(WO_3)_3PO_3CH_3$, $Rb_2(WO_3)_3PO_3CH_3$ and $(NH_4)_2(WO_3)_3PO_3CH_3$ have been prepared for the first time and structurally and physically characterized. They are non-centrosymmetric layered phases isostructural with their molybdenum(VI)-containing analogues $Cs_2(MoO_3)_3PO_3CH_3$ and $Rb_2(MoO_3)_3PO_3CH_3$.[3] A polyhedral view of this structure type is shown in Fig. 12. Powder neutron diffraction was successful in elucidating the full structure, including the hydrogen atom position in $Cs_2(WO_3)_3PO_3CH_3$. A three-layer (ABCABC ...) repeat motif in the *c* direction is observed in these structures: as with the $M_2(MoO_3)_3PO_3CH_3$ structures, this may be correlated with the steric requirements of the methylphosphonate group, which points towards a six-ring window in each adjacent sheet.[3] Because of the staggered stacking arrangement of the $(WO_3)_3PO_3CH_3$ sheets in these structures, there are no pseudo-infinite channels comparable to the six-ring channels found in hexagonal WO_3.[15]

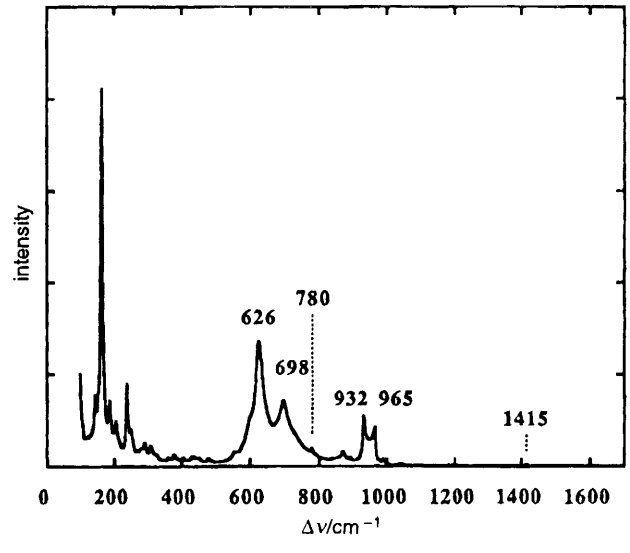

Fig. 11 Raman spectrum of $Cs_2(WO_3)_3PO_3CH_3$

The distortion mode of the octahedral cation is different for the tungsten and molybdenum phases: in the $M_2(MoO_3)_3PO_3CH_3$ materials, the Mo atom displacement inside the MoO_6 octahedron is towards an octahedral face [so-called local (111) distortion], resulting in a (three short + three long) Mo—O bond distance distribution in both $Cs_2(MoO_3)_3PO_3CH_3$ [$\Delta_{Oct}=0.34$ Å] and $Rb_2(MoO_3)_3PO_3CH_3$ [$\Delta_{Oct}=0.34$ Å]. However, in $Cs_2(WO_3)_3PO_3CH_3$, the W atom displacement is towards an octahedral edge [local (110) distortion], and the WO_6 bonding situation described above results.

Compounds $Cs_2(WO_3)_3PO_3CH_3$, $Rb_2(WO_3)_3PO_3CH_3$ and $(NH_4)_2(WO_3)_3PO_3CH_3$ complement the layered tungsten(VI) selenites $(NH_4)_2(WO_3)_3SeO_3$ and $Cs_2(WO_3)_3SeO_3$.[5] However, in the two-layer (ABAB ...) selenite phases, the tungsten atom displays a local [111] distortion mode inside its oxygen atom octahedron [for $(NH_4)_2(WO_3)_3SeO_3$, $\Delta=0.20$ Å; for $Cs_2(WO_3)_3SeO_3$, $\Delta=0.27$ Å], similar to the bonding situation for the molybdenum methylphosphonates.

The displacement of a Mo^{VI} or W^{VI} d^0 cation in octahedral coordination may be understood in terms of a second-order Jahn–Teller effect:[18] 'spontaneous' distortion of the MoO_6 or WO_6 unit will remove degeneracies in the molecular energy levels which arise from overlap of the unoccupied d orbitals of the metal species with the filled p orbitals of the oxygen atom species. The smaller distortion (off-centre displacement of the W atoms) in the tungsten compound is consistent with the general observation that distortions around d^0 transition metals increase with increasing cation charge, but decrease with increasing cation size.[19] The magnitude and direction of the cation displacement inside the octahedron is much harder to predict from first principles, and may reflect a combination of second-order electronic effects, lattice stresses, and cation–cation repulsions, as discussed recently by Kunz and Brown.[19]

The layer separation (defined by the separation of the W atoms in the *z* direction) for $Cs_2(WO_3)_3PO_3CH_3$ is 6.76 Å, with a comparable value of 6.45 Å for $(NH_4)_2(WO_3)_3PO_3CH_3$. This suggests that the cation plays some role in defining the interlayer separation in these tungsten-containing phases. Conversely, in the $M_2(MoO_3)_3PO_3CH_3$ phases, the *c* unit-cell dimension is almost identical for both the caesium and rubidium congeners,[3] suggesting that interlayer packing considerations are most important for the Mo-containing materials.

The various layered HTO-type phases are summarized in

Table 6 Summary of layered HTO-type phases

formula	a/Å	c/Å	V/Å^3	space group	ref.
$SrAl_3(OH)_6(PO_4)(HPO_4)$	7.015(3)	16.558(6)	705.7	$R\bar{3}m$	7
$KAl_3(OH)_6(SO_4)_2$[a]	7.020(2)	17.223(8)	735.0	$R\bar{3}m$	8
$NaAl_3(OH)_6(CrO_4)_2$	7.060(3)	17.25(2)	744.6	$R\bar{3}m$	9
$Ga_3(OH)_6(SO_4)(HSO_4)\cdot H_2O$	7.178	17.170	766.1	$R\bar{3}m$	10
$KFe_3(OH)_6(SO_4)_2$	7.315(2)	17.224(6)	798.2	$R\bar{3}m$	8
$K_3(SbO_2)_3(PO_4)_2\cdot nH_2O$	7.147(1)	30.936(6)	1368.5	$R\bar{3}m$	11
$K(VO_2)_3(SeO_3)_2$	7.125(4)	11.414(3)	501.8(5)	$P6_3$	4
$Rb(VO_2)_3(SeO_3)_2$	7.131(1)	11.459(6)	504.6(9)	$P6_3$	20
$NH_4(VO_2)_3(SeO_3)_2$	7.137(3)	11.462(4)	505.7(4)	$P6_3$	1
$Tl_2(MoO_3)_3SeO_3$	7.2774(5)	11.785(2)	540.5(1)	$P6_3$	21
$Rb_2(MoO_3)_3SeO_3$	7.283(4)	11.964(8)	549.6(8)	$P6_3$	21
$(NH_4)_2(MoO_3)_3SeO_3$	7.267(2)	12.031(3)	550.3(3)	$P6_3$	2
$Cs_2(MoO_3)_3SeO_3$	7.312(2)	12.377(2)	573.1(3)	$P6_3$	2
$Rb_2(WO_3)_3SeO_3$	7.2834(4)	11.965(1)	549.7	$P6_3$	5
$(NH_4)_2(WO_3)_3SeO_3$	7.2291(2)	12.1486(3)	549.82(3)	$P6_3$	5
$Cs_2(WO_3)_3SeO_3$	7.2615(2)	12.5426(3)	572.75(3)	$P6_3$	5
$Cs_2(MoO_3)_3PO_3CH_3$	7.304(2)	20.02(1)	924.7	$R3$	3
$Rb_2(MoO_3)_3PO_3CH_3$	7.307(2)	20.040(4)	926.7	$R3$	3
$(NH_4)_2(WO_3)_3PO_3CH_3$	7.22851(7)	19.3471(3)	875.48(3)	$R3$	this work
$Rb_2(WO_3)_3PO_3CH_3$	7.2483(5)	19.3034(6)	878.30	$R3$	this work
$Cs_2(WO_3)_3PO_3CH_3$	7.25791(9)	20.2762(4)	925.00(4)	$R3$	this work

[a] Various other complex alunite-type [$KAl_3(OH)_6(SO_4)_2$-type] minerals also exist.

Table 6. All these phases have hexagonal (trigonal) a and b unit-cell parameters of *ca.* 7.0–7.3 Å, as does hexagonal WO_3 itself[6] (a = 7.298 Å). Their c unit-cell dimensions vary depending on the capping group, the layer-repeat motif, and the type of interlayer species. The phases reported earlier[7–11] are all capped on both faces of the octahedral sheets by tetrahedral groups, and all crystallize in the centrosymmetric space group $R\bar{3}m$. They all consist of three-layer (ABCABC ...) repeat motifs in the c unit-cell direction. The much larger c unit-cell parameter observed for the potassium antimony phosphate hydrate phase,[11] compared to the alunite-type [$KAl_3(OH)_6(SO_4)_2$] phases,[7–10] arises from the different arrangement of the interlayer K/H_2O species in the former material. The new HTO-type phases[1–5] all crystallize in non-centrosymmetric space groups and may adopt double (vanadium-containing phases) or single (molybdenum, tungsten) capping as noted above in the introduction.

We thank Paul Meloni and Roman Czernuszewicz for assistance in collecting the Raman data. This work was funded by the National Science Foundation (DMR9214804) and the Robert A. Welch Foundation (E-1207). The neutron diffraction experiments were supported by the Division of Materials Sciences, US Department of Energy, under contract no. DEA-AC02-76CH00016.

References

1 J. T. Vaughey, W. T. A. Harrison, L. L. Dussack and A. J. Jacobson, *Inorg. Chem.*, 1994, **33**, 4370.
2 W. T. A. Harrison, L. L. Dussack and A. J. Jacobson, *Inorg. Chem.*, 1994, **33**, 6043.
3 W. T. A. Harrison, L. L. Dussack and A. J. Jacobson, *Inorg. Chem.*, 1995, **34**, 4774.
4 W. T. A. Harrison, L. L. Dussack and A. J. Jacobson, *Acta Crystallogr., Sect. C*, 1995, in the press.
5 W. T. A. Harrison, L. L. Dussack, T. Vogt and A. J. Jacobson, *J. Solid State Chem.*, 1995, in press.
6 B. Gérand, G. Nowogrocki, J. Guenot and M. Figlarz, *J. Solid State Chem.*, 1979, **29**, 429.
7 T. Kato, *Mineral. J.*, 1987, **13**, 390.
8 S. Menschetti and C. Sabelli, *Neues Jahrb. Mineral Monatsh.*, 1976, 406.
9 Y. Cudennuc, A. Riou and A. Bonnin, *Rev. Chim. Miner.*, 1980, **17**, 1158.
10 G. Johannson, *Ark. Kemi*, 1963, **20**, 343.
11 M. Tournoux, M. Ganne and Y. Piffard, *J. Solid State Chem.*, 1992, **96**, 141.
12 A. C. Larson and R. B. Von Dreele, *GSAS User Guide*, Los Alamos National Laboratory, Los Alamos, New Mexico, USA, 1991.
13 C. J. Howard, *J. Appl. Crystallogr.*, 1982, **15**, 615.
14 N. E. Brese and M. O'Keeffe, *Acta Crystallogr., Sect. B*, 1991, **47**, 192.
15 B. Gérand, G. Nowogrocki, J. Guenot and M. Figlarz, *J. Solid State Chem.*, 1979, **29**, 429.
16 R. Diehl, G. Brandt and E. Salje, *Acta Crystallogr., Sect. B*, 1978, **34**, 1105.
17 W. Kwak, M. T. Pope and T. F. Scully, *J. Am. Chem. Soc.*, 1975, **97**, 5735.
18 J. K. Burdett, *Molecular Shapes*, Wiley, New York, 1980.
19 M. Kunz and I. D. Brown, *J. Solid State Chem.*, 1995, **115**, 395.
20 L. L. Dussack, W. T. A. Harrison and A. J. Jacobson, unpublished results.
21 L. L. Dussack, W. T. A. Harrison and A. J. Jacobson, *Mater. Res. Bull.*, 1996, in press.

Paper 5/03853G; *Received* 14*th June*, 1995